Novel Electrolytes for Aluminium-Sulfur Batteries: Critical Evaluation of Electrode Thickness Effects and Side Reactions

John Lampkin‡[a], He Li‡[a], Liam Furness[a], Rinaldo Raccichini[a],[b] and Nuria Garcia-Araez*[a]

[a] Dr. J. Lampkin, Dr. H. Li, L. Furness, Dr. R. Raccichini, Prof. N. Garcia-Araez
School of Chemistry, University of Southampton
University Road, Southampton, SO17 1BJ, United Kingdom
E-mail: n.garcia-araez@soton.ac.uk
[b] Dr. R. Raccichini
National Physical Laboratory (current address)
Hampton Road, Teddington, Middlesex, TW11 0LW, United Kingdom
‡ These authors contributed equally to this work.

Supporting information for this article is given via a link at the end of the document.

Abstract: The high abundance and low cost of aluminium and sulfur make the Al-S battery an attractive combination. However, significant improvements in performance are required, and increasing the thickness and sulfur content of the sulfur electrodes is critical to develop batteries with competitive values of specific energy. This work reports the development of sulfur electrodes with the highest sulfur content (60% wt.) reported to date for the Al-S battery system, and presents a systematic study of the effect of the sulfur electrode thickness on battery performance. When using low cost electrolytes made with acetamide or urea, the slow mass transport of electrolyte species is identified as the main cause of the poor sulfur utilisation when increasing the electrode thickness, whereas complete sulfur utilisation is achieved with a less viscous ionic liquid. In addition, the analysis of very thin electrodes reveals the occurrence of degradation reactions in the low cost electrolytes. In summary, the new method of analysis here developed is ideally suited to evaluate the stability and mass transport limitations of novel electrolytes for Al-S batteries.

Introduction

Lithium-ion batteries are currently the best performing rechargeable battery on the market, used in mobile devices, electric vehicles and various other small-scale energy storage solutions. As the demand for cheaper batteries with larger energy capacity increases, researchers are turning towards alternatives and developing new battery systems. Many factors are contributing to this, including the limited lithium natural resources,[1] the flammable nature of the organic-based solvent,[2] the limited practical specific energy achievable by lithium-ion batteries and difficulty of recycling.[3]

A variety of battery technologies will be required to meet the energy storage needs in coming years, and the aluminium-sulfur battery is likely to play an important role, since it is made of cheap and highly abundant elements and it can potentially achieve very high values of energy per unit mass or volume. Aluminium as an anode material has high abundance and very high theoretical values of gravimetric and volumetric capacity (2980 mAh g^{-1} and 8040 mAh cm^{-3} respectively).[4] Coupling an aluminium anode with a sulfur cathode, another abundant material, produces a battery with a theoretical voltage of ca. 1.23 V, high theoretical specific energy (1319 Wh kg^{-1}) and high theoretical energy density (2981 Wh L^{-1}).[5]

Table 1 presents a summary of all published research articles on Al-S battery development to date. It is clear that the Al-S battery is in its infancy, but promising high values of specific capacity have been achieved. These early studies demonstrate the potential of Al-S batteries as an alternative low cost battery, but much more work is required to improve performance to pave the way towards commercialisation.[5] Table 1 shows that all previous studies have been done with very low loadings of sulfur in the cathode (which is defined as the mass of sulfur per geometrical area of the cathode). In addition, the sulfur content in the cathode (% of the total mass of the cathode coating that is sulfur) is also rather low. However, sulfur electrodes with high sulfur loading and high sulfur content are required to meet the requirements of commercial applications of high specific energy and high energy density. To illustrate this point we include in table 1 the calculation of the specific energy of the cells normalized by the total mass of the sulfur and aluminium electrodes. Although these values are still promising, further decreases in specific energy will occur due to the mass of passive components (electrolyte, current collectors, etc.), but the effect of the latter will be minimized by increasing the mass fraction of the active materials in the battery by increasing the sulfur loading in the sulfur electrode.[6]

This work presents a systematic study of the effect of sulfur loading on the performance of Al-S batteries, which enables the identification of the critical issues that need to be addressed for the development of Al-S batteries to meet the requirements towards commercialization. The measurements were done with advanced cathode formulations containing a relatively high sulfur content (~60 % wt.), which is the highest reported in the literature to date for the Al-S battery system. The cathodes were prepared by doctor blade coating a thick slurry on an inert Mo foil, since Mo is a stable material in Al-ion electrolytes.[7] All the materials employed in the electrochemical cells were carefully selected to be resistant against degradation in contact with the corrosive Al-ion electrolytes. Three different types of electrolytes have been selected for this study, which provides new, unprecedented understanding into the reaction mechanism and differences in chemical stability of the different electrolytes in Al-S battery reactions.

Table 1. Comparison of the main electrochemical results reported in Al-S battery studies, in chronological order (from older to newer)

Work	Electrode Composition	Electrolyte	Sulfur Content (% wt.)	Sulfur Loading (mg cm^{-2})	Specific Current (mA g_S^{-1})	Initial Specific Discharge Capacity (mAh g_S^{-1})	Discharge Voltage (V)[a]	Specific Energy of Initial Discharge (Wh $kg_{electrodes}^{-1}$)[b]
G. Cohn et. al, 2015[8]	S, Ketjen black, PVDF (50:30:20) on stainless steel (non-rechargeable)	EMICl-$AlCl_3$ (1:1.5)	50	1.1	30	1400	1.2	656
T. Gao et. al, 2016[4a]	S on activated carbon cloth	EMICl-$AlCl_3$ (1:1.3)	n/a	0.8-1.0	50	1320	0.65	n/a
X. Yu et. al, 2017[9]	Spreading the mixture of S and ionic liquid electrolyte onto activated CNF paper (S:CNF≈1:2)	EMICl-$AlCl_3$ (1:1.3)	33	~1.0	~30 (C/50)	1350	1.05	395
X. Yu et. al, 2018[10]	Spreading the mixture of S and ionic liquid electrolyte onto activated CNF paper (S:CNF≈1:2)	0.5 M $LiCF_3SO_3$ in EMICl-$AlCl_3$ (1:1.25)	33	~1.0	~30 (C/50)	1250	0.76	265
H. Yang et. al, 2018[11]	S, CMK-3, Ketjen black, PTFE (40:40:10:10)	EMIBr-$AlCl_3$ (1:1.3)	40	n/a	251	1500	~0.5	245
		NBMPBr-$AlCl_3$ (1:1.3)	40	n/a	251	1390	~0.5	227
Y. Bian et. al, 2018[12]	S, MWCNT, polyacrylic latex (10:80:10) on Ni foil	Urea-$AlCl_3$ (1:1.4)	10	0.42	1000	740	~1.7	119
W. Wang et. al, 2018[13]	10 % S. SPAN, Ketjenblack and PTFE (80:10:10) on carbon paper.	EMICl-$AlCl_3$ (1:1.5)	10	0.12	25	320	0.3	9
W. Chu et. al, 2019[14]	S, CMK-3 1:1, with 10 % PTFE and 10 % Super C on Mo foil	Acetamide-$AlCl_3$ (1:1.3)	40	0.25	100	2100	0.55	377
K. Zhang et. al, 2019[15]	BN/S/C (6:1:2) with 10 % PVDF coated on Pt coated OHP organic film	EMICl-$AlCl_3$ (1:1.3)	10	~0.3	100	~275	1.15	~30
This work	S, CNT with PEO and PVP coated on Mo foil (58.8:29.4:7.9:3.9)	EMICl-$AlCl_3$ (1:1.5)	58.8	~0.4-3.5	50	1404[c]	0.31	192
		Acetamide-$AlCl_3$ (1:1.5)	58.8	~0.4-3.5	50	2129[c]	0.42	395
		Urea-$AlCl_3$ (1:1.5)	58.8	~0.4-3.5	50	2359[c]	0.41	428

[a] The discharge voltage from this work is the average voltage calculated by integrating the discharge voltage over the discharge capacity and then dividing by the total discharge capacity. The calculation procedure can be found in the Supplementary Information (Equation S1). Since the average voltage has not been reported in previous published papers, the discharge voltage plateau is reported instead.
[b] The specific energy of the initial discharge is normalized to the total mass of the sulfur and aluminium electrodes, and the calculation procedure can be found in the Supplementary Information (Equation S2).
[c] The thinnest mass loading (~0.4 mg cm^{-2}) is used when reporting the specific capacity and specific energy.

The first electrolyte selected for this study is the most commonly used electrolyte in Al-S batteries: the ionic liquid EMIMCl-$AlCl_3$. It is made by mixing $AlCl_3$ with an organic cation chloride salt, namely 1-ethyl-3-methylimidazolium chloride (EMIMCl). $AlCl_3$ is a Lewis acid that is added in excess to facilitate reversible electrochemical process of Al stripping/plating;[16] here a molar ratio of EMIMCl:$AlCl_3$ of 1:1.5 is used, which results in an electrolyte containing equimolar concentrations of $AlCl_4^-$ and $Al_2Cl_7^-$.[17]

The other two electrolytes used here are deep eutectic solvents made by mixing a Lewis base with $AlCl_3$, where $AlCl_3$ is added in excess, again to facilitate reversible Al electrochemistry. Deep eutectic solvents have a significant cost advantage over ionic liquids, while the conductivity and suitability for Al plating/stripping reactions is maintained.[18] Here we use either acetamide or urea as the Lewis base, and the resulting electrolytes are called Acetalumina (acetamide: $AlCl_3$ in a 1:1.5 molar ratio) and Uralumina (urea: $AlCl_3$ in a 1:1.5 molar ratio). The actual species present in the deep eutectic solvents are thought to be a mixture of aluminium species complexed with chloride anions and acetamide/urea ligands.[19]

The evaluation of the Al-S battery electrochemical performance as a function of sulfur loading here presented demonstrates that, unfortunately, the chemical stability of the chosen deep eutectic solvents is currently insufficient for Al-S battery applications, whereas the ionic liquid EMIMCl-$AlCl_3$ appears to be much more stable. Further work is required to explore other deep eutectic solvent formulations with improved chemical stability. In addition, it is found that the high viscosity of these aluminium electrolytes is a very important factor affecting performance at increasing sulfur loadings. Thus, further work is required for the development of less viscous electrolytes and advanced cathode structures with controlled porosity and low tortuosity to enable fast electrolyte ion transport.

Results and Discussion

Increasing the amount of sulfur in Al-S batteries is crucial for achieving high energy from a light battery, thus, increasing the sulfur content and loading in the cathode is essential. This work reports a systematic study of the effect of sulfur loading in cathodes containing a high sulfur content of ~60 %. Increasing the sulfur loading is achieved by increasing the mass of cathode loaded onto a Mo thin film substrate by increasing the wet thickness in the doctor blading coating process. This also produces an increase in the cathode thickness, which is measured using a high-precision thickness gauge.

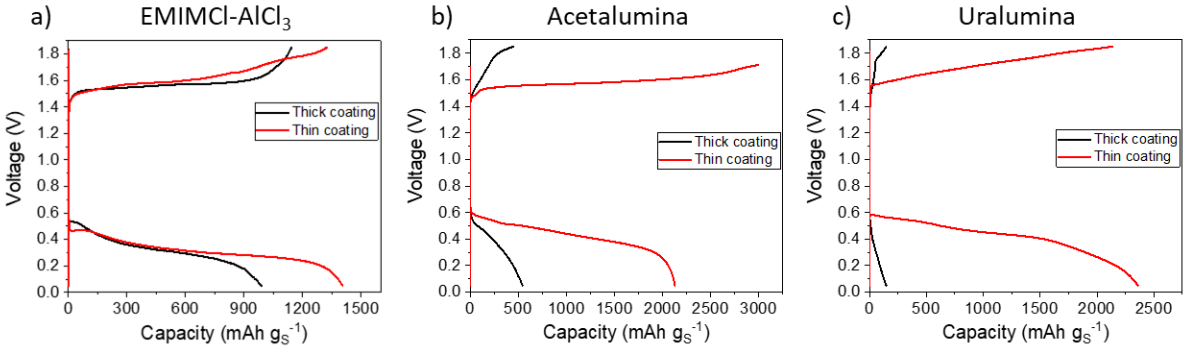

Figure 1. 1st cycle voltage profiles of thick (139 µm) and thin (22 µm) cathode coatings when using a) EMIMCl-$AlCl_3$, b) Acetalumina and c) Uralumina electrolytes. Experiments used a specific current of 50 mA g_S^{-1} and a 0.05-1.85 V voltage range. Cathodes contain 60 % sulfur and CNT as conductive additive.

Figure 1 illustrates the effect of increasing the cathode thickness on the electrochemical performance of Al-S batteries containing the three different electrolytes. Note that low cathode loadings have been prepared using a thinner Mo foil substrate, which enables an accurate evaluation of the cathode coating mass (see details in the experimental section). This enables the reliable determination of the sulfur mass loading, which is required for normalizing the capacity values. Note also that reversible Al plating/stripping was achieved in all electrolytes (see cycling of Al-Al symmetrical cells in Figure S1), in agreement with previous work.[16b, 16c, 17a, 18] And also note that the selected voltage window avoids the oxidation of the electrolyte at ≥ 2 V (Figure S2), in agreement with previous studies.[20]

Figure 1 shows that increasing the sulfur loading dramatically affects the electrochemical response in the deep eutectic solvents Acetalumina and Uralumina, while for the ionic liquid EMIMCl-$AlCl_3$, the effect of sulfur loading is much more moderate. This behaviour can be understood in view of the viscosities of the different electrolytes, as shown in Table 2 (see details of calculations in the supplementary information, Equation S3). The viscosity increases dramatically in the order EMIMCl-$AlCl_3$ < Acetalumina < Uralumina, and the decrease in capacity for thick cathode coatings increases in the same way.

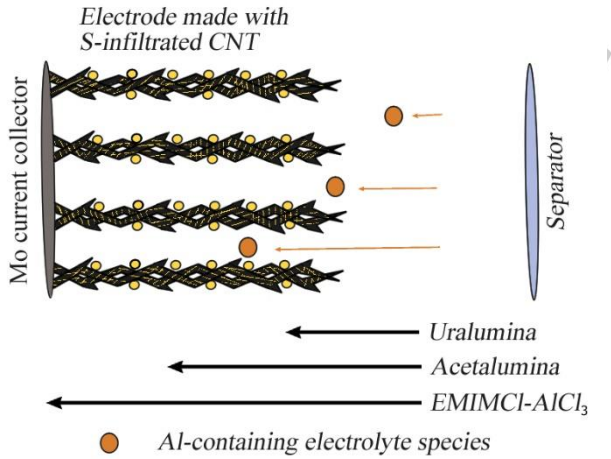

Figure 2. Illustration of the limitations due to slow transport of Al-containing electrolyte species within the porous sulfur cathode in Al-S cells.

Consequently, it can be proposed that for the highly viscous electrolytes, mass transport limitations severely affect the performance and, consequently, only a small fraction of the sulfur present in the cathode participates in the electrochemical reactions, thus producing very small specific capacities. Figure 2 illustrates that, for slow transport of aluminium-containing species within the electrolyte filling the cathode pores, most of the reaction will take place in cathode regions that are closer to the separator, and the regions closer to the current collector will become underutilised. Since the reduction of sulfur produces Al_2S_3, which is an insulating solid, as the reaction proceeds, deposition of Al_2S_3 can block some of the pores of the sulfur composite cathode, thus slowing down mass transport and making some of the regions of the cathode poorly accessible. With faster mass transport, the reaction would be more homogeneous and the whole electrode could participate in the electrochemical reactions.

Table 2. Viscosity of electrolytes at room temperature (ca. 20 °C)

Substance	EMIMCl-$AlCl_3$	Acetalumina	Uralumina
Density /g mL^{-1}	1.360	1.460	1.564
Time /s	98	643	1398
Viscosity /mPa s	13	94	218

Figure 3 shows the experimental first discharge specific capacities, obtained for a variety of cathode thicknesses and cathode formulations, plotted against the sulfur loading of the cathode (a,b,c) or the cathode thickness (d,e,f). The data gathered for these graphs is comprised of between 35-43 individual experiments per electrolyte. It is clear that for Acetalumina, and especially for Uralumina, a marked decrease in specific capacity is observed as the cathode is deposited as a thicker coating on the Mo thin film substrate. Conversely, in the ionic liquid EMIMCl-$AlCl_3$, the effect of cathode thickness is much less marked. These findings give further support to the hypothesis that the full utilisation of thick electrodes in highly viscous electrolytes is difficult due to mass transport limitations, which are exacerbated in Al-S batteries due to the fact that the discharge product Al_2S_3 can clog the cathode pores. Interestingly, mass transport limitations have also been identified as a major issue limiting the capacity of state-of-the-art Li-S cells.[21]

To summarise, achieving high specific capacities with high sulfur loading cathodes requires the development of advanced cathode morphologies able to facilitate fast transport of Al-containing electrolyte species through the whole porous cathode. For the cathodes here developed, the SEM images of thin and thick electrodes (Figure 4) show the presence of agglomerates and cracks. The thicker coating contains large cracks (Figure 4c)

that can also be observed directly by eye. Upon magnification, the SEM images show the presence of coating material at the bottom of the cracks (Figure 4d), suggesting that the cracks are formed during drying of the ink deposit. This is in line with previous studies on the development of advanced cathodes for Li-S batteries, which showed that special combinations of different carbons and binders were required to produce thick sulfur cathode composites with good mechanical stability, no substantial cracking and good electrochemical performance.[22] On the other hand, elemental analysis of the cathodes by EDS (Figure 5) shows homogeneous distribution of sulfur and carbon, which could be attributed to the step of sulfur infiltration on the carbon nanotubes prior to the preparation of the electrodes.

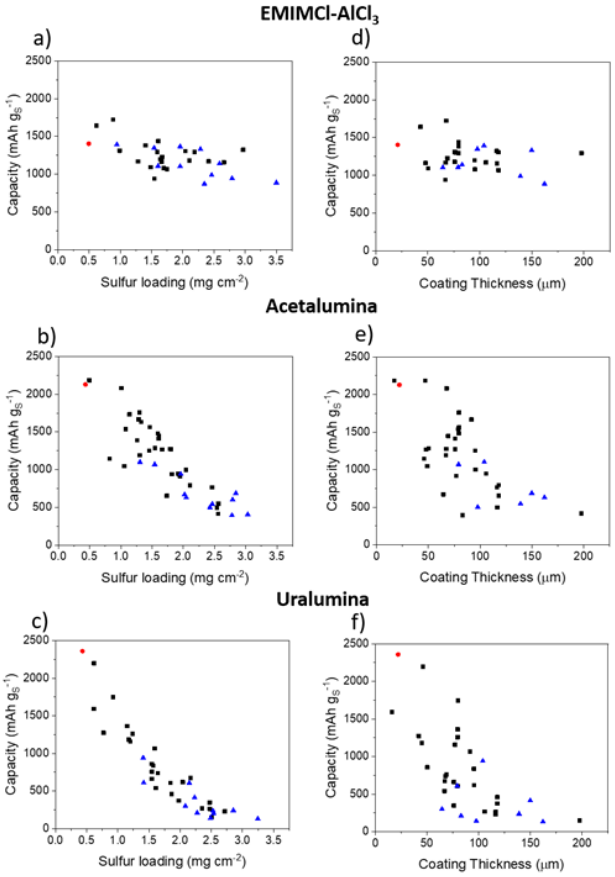

Figure 3. 1st discharge capacity values plotted against the sulfur loading (a, b, c) or the cathode coating thickness (d, e, f) in EMIMCl-$AlCl_3$ (a, d), Acetalumina (b, e), and Uralumina (c, f). The black square symbols show the results obtained with the electrodes coated on a thicker (25 µm) Mo foil, while the red circle points show the results using a thinner (10 µm) Mo foil. In both cases, the electrodes contain 60 % sulfur and CNT as the only carbon source. The blue triangle points show the results of electrodes made with a small amount (1-8 %) of other carbon additives mixed with CNT.

A quantitative analysis of electrolyte ion transport within the porous sulfur cathode was done for the Uralumina electrolyte with impedance measurements of the sulfur electrodes in symmetrical cells (Figure 6). These measurements were done in a cell containing two nearly identical cathodes, and therefore, the impedance of the cell is simply two times the impedance of one cathode.[23] By contrast, when impedance measurements are done in Al-S cells, it is difficult to separate the contributions due to the impedance of the aluminium anode and the sulfur cathode. The impedance results in Figure 6 show a depressed semi-circle that is caused by the contact resistance with the current collector, and can be fitted to a resistor and a CPE element in parallel.[23a, 24] This is followed by a 45-degree line reflecting the transport of electrolyte ions through the porous electrodes, and then a vertical line reflecting the capacitative behaviour of the electrode at low frequencies where only double-layer charging of the carbon-electrolyte interphase takes place. Note that charge-transfer reactions of sulfur reduction to polysulfides are absent in these measurements because the sulfur electrodes are at a high potential (around 1.3 V vs. Al).

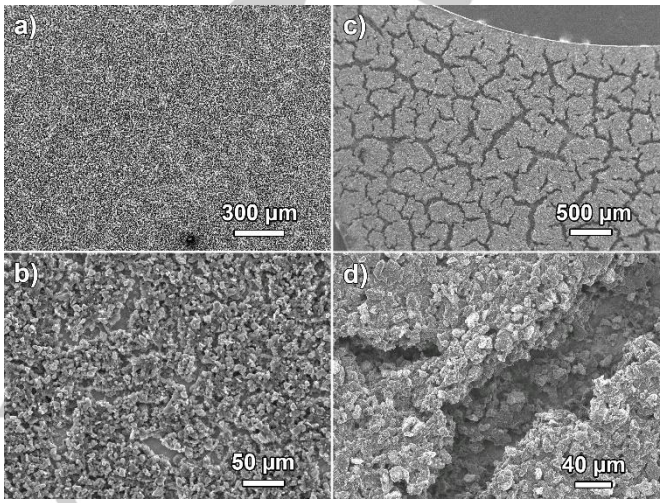

Figure 4. SEM images of sulfur electrodes of thin coating (a and b, ~45 µm cathode layer) and thick coating (c and d, ~80 µm cathode layer), taken before cell assembly and cycling. a and c are at low magnification while b and d are at high magnification.

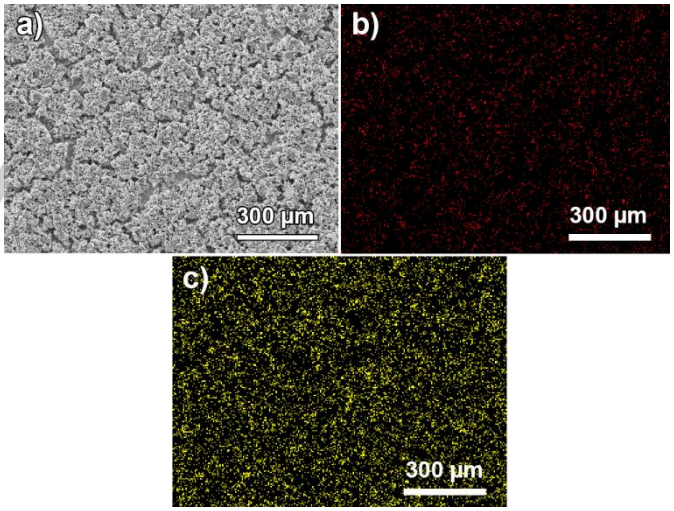

Figure 5. EDS maps of a sulfur cathode coating of 60 µm thickness. SEM image (a) and associated distribution of carbon (b, red) and sulfur (c, yellow).

Figure 6 shows that the length of the 45-degree line (which measures the resistance associated to electrolyte ion transport within the porous electrode) increases as the electrode becomes thicker. This support the hypothesis that increasing the electrode thickness produces more severe mass transport limitations in highly viscous electroltyes. The results can be fitted to the equivalent circuit shown in the figure, in which an open Warburg element is used to describe the transport of electrolyte ions through the pores of the electrode coupled to double-layer charging at the carbon-electrolyte interphase.[23a] The analysis of

the data is described in the supporting information (Equations S4 and S5) and the results of the analysis are summarized in Table 3. The analysis enables the evaluation of an effective tortuosity, which is a measure of the ratio between the ion transport path length and the geometrical thickness of the electrodes: higher tortuosity denotes a more intricate pathway and slower ion transport. Table 3 shows that, despite the high porosity of the electrodes here employed, the tortuosity towards ion transport is rather high, which can be attributed, at least in part, to the formation of dense agglomerates and cracks in the electrodes. Further work will exploit the use of impedance measurements of sulfur composite electrodes in symmetrical cells to support the rational development of electrode/electrolyte formulations producing fast ion transport (that is, low Warburg resistance), and thus, with potential to deliver high specific capacity for electrode thicknesses relevant to commercial applications.

Coming back to the electrochemical results, close inspection of Figures 1 and 3 also show that for Acetalumina and Uralumina, low cathode loadings produce very high values of specific capacity, much higher than the theoretical capacity of 1672 mAh g^{-1} associated to the full reduction of sulfur to sulfide. Two previous studies of Al-S batteries reported values of specific capacity higher than the theoretical limit. The first one reported 1750 mAh g_S^{-1} in an EMIMCl-$AlCl_3$ electrolyte at 50 °C and the second one reported 2100 mAh g_S^{-1} in an Acetalumina electrolyte at room temperature.[4a, 14] In both cases, it was argued that the high values of capacity could be due to capacity contributions from carbon or to side reactions, without providing any additional experimental evidence.

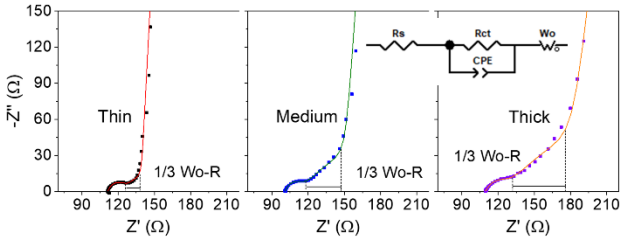

Figure 6. Nyquist plots of symmetrical cells containing thin (~60 µm), medium (~120 µm) and thick (~190 µm) sulfur cathode coatings in Uralumina. A 10 mV perturbation with a frequency range 200 kHz – 10 mHz was used. The line shows the length of the 45-degree line representing one third of the total resistance due to electrolyte ion transport through the porous electrode.

In order to evaluate the contribution of the carbon conductive additive to the specific capacity of the sulfur cathodes, additional experiments were performed with electrodes containing the carbon conductive additive and no sulfur. Figure 7 shows the voltage profile obtained with composite electrodes containing CNT and binder only (without any sulfur), when cycling against an aluminium counter-electrode, for the three electrolytes under study (note that values of specific capacity in Figure 7 are normalized to the mass of carbon in the electrodes). The sulfur cathodes used in this work (Figures 1 and 3) had a ratio of carbon and sulfur mass content of 0.5 g_c/g_s, and since the applied specific current (normalized to the mass of sulfur) was 50 mA g_S^{-1}, then the value of specific current normalized to the mass of carbon is 100 mA g_c^{-1}. For that reason, the electrodes in Figure 7 were cycled with a specific current of 100 mA g_C^{-1}. In addition, the electrodes were prepared with a loading of ca. 0.3 mg_c cm^{-2} to facilitate the full utilisation of all the carbon present in the electrodes in the electrochemical reactions (for comparison, the carbon loadings in the sulfur cathodes used in Figures 1 and 3 were between 0.2 and 1.75 mg_c cm^{-2}).

Table 3. Summary of the results of the analysis of the impedance measurements in Figure 6. The errors reported are obtained from the impedance fitting and propagation of experimental errors.

Electrode	Thin ~60 µm	Medium ~120 µm	Thick ~190 µm
R_s (Ω)	111.2 ± 0.2	100.6 ± 0.1	109.1 ± 0.3
CPE-T (F s^{P-1})	(6.5 ± 2.1)x10^{-5}	(8.4 ± 1.9)x10^{-5}	(1.02 ± 0.45)x10^{-4}
CPE-P	0.955 ± 0.042	0.982 ± 0.031	0.909 ± 0.060
R_{ct} (Ω)	11.6 ± 0.5	10.8 ± 0.3	12.0 ± 0.7
Wo-R (Ω)	47.9 ± 1.8	114.7 ± 1.5	173.8 ± 3.6
Wo-T (s)	0.160 ±0.007	0.707 ± 0.011	0.730 ± 0.018
Wo-P	0.484 ± 0.005	0.479 ± 0.001	0.466 ± 0.001
Porosity (%)	81±6	82±3	88±2
MacMullin Number	4.0±0.3	4.8±0.2	4.6±0.2
Tortuosity	3.2±0.4	3.9±0.2	4.1±0.2

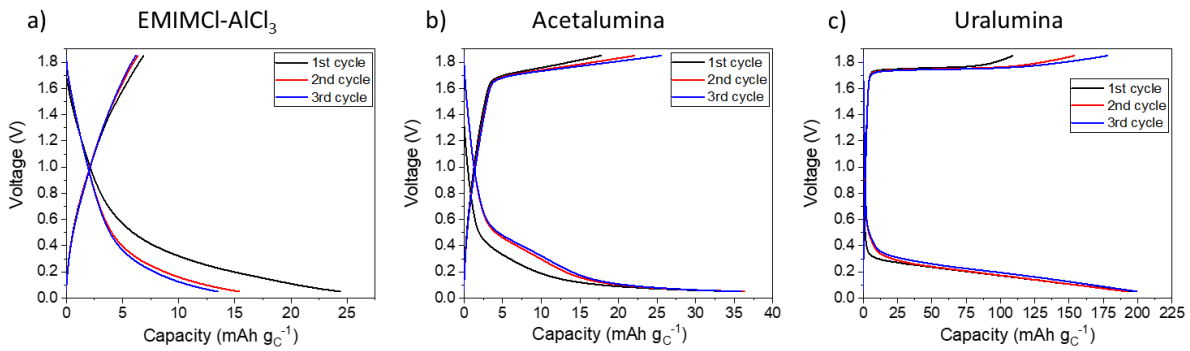

Figure 7. 1st cycle voltage profile of cathodes made with only CNT and binder using a) EMIMCl-$AlCl_3$, b) Acetalumina and c) Uralumina electrolytes. Experiments used a specific current of 100 mA g_c^{-1} and the voltage range is 0.05-1.85 V.

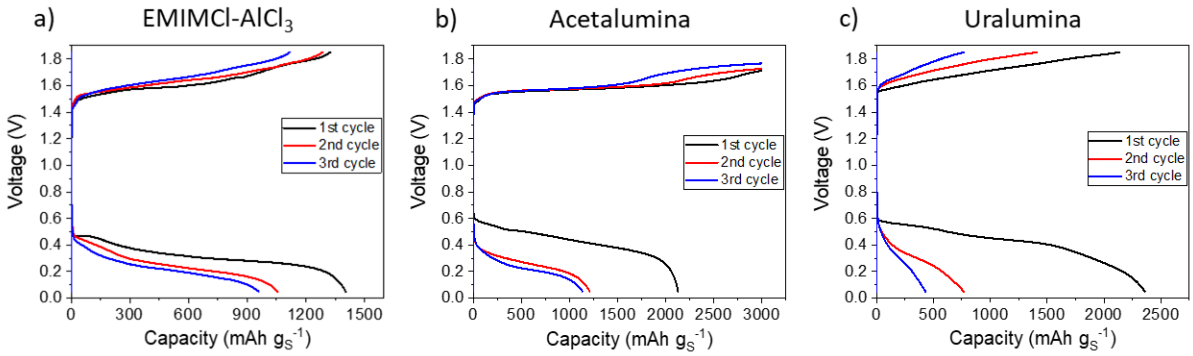

Figure 8. First three galvanostatic cycles of the thin cathode coatings shown in Figure 1.

The results in Figure 7 clearly show that very small specific capacities were obtained with electrodes containing only carbon and binder. This demonstrates that electrochemical reactions taking place on the carbon conductive additive of sulfur cathodes produce a very small contribution to the total capacity. The same argument can be made by simply comparing the experimental capacities, without normalization to the mass of either sulfur or carbon. The capacities obtained with cells with carbon-only electrodes (Figure 7) were 12, 15 and 84 µAh in EMIM-$AlCl_3$, Acetalumina and Uralumina electrolytes, respectively, whereas with the thin electrodes with sulfur (Figure 1) the capacities were 660, 876 and 971 µAh. This demonstrates that the contribution of the carbon response to the experimental capacities of the sulfur cathodes here developed is only minor.

Consequently, the fact that the experimental capacities are higher than the theoretical limit of 1672 mAh g_S^{-1} can only be explained by the fact that side reactions (most likely, electrolyte degradation) are also involved in the discharge of the batteries. While each sulfur atom can only receive a maximum of two electrons (which produces the theoretical capacity of 1672 mAh g_S^{-1}), additional processes can be induced during the discharge of the battery that can consume more electrons, such as, for instance, the reduction of urea or acetamide. Such degradation of the electrolyte is not observed in the electrodes without sulfur (Figure 7), which suggests that polysulfide species formed in the pathway of sulfur reduction to sulfide are the triggers of the degradation reactions. Conversely, it is interesting to see that the ionic liquid EMIMCl-$AlCl_3$ does not produce capacities exceeding the theoretical limit, which suggests that this electrolyte is stable, at least under the experimental conditions employed here.

Figure 8 shows the evolution of the voltage profiles of Al-S cells during the first 3 cycles. Perhaps as a result of the degradation reactions discussed above, the discharge voltage and discharge capacity in Uralumina and Acetalumina markedly decreases with cycling. On the other hand, the cycling stability in EMIMCl-$AlCl_3$ is much better, but still major improvements are required to meet the requirements for commercial applications. Figure 9 shows the variation of the discharge capacity with cycling, again showing marked decreases with cycling in the deep eutectic electrolytes and better capacity retention in the ionic liquid EMIMCl-$AlCl_3$.

Finally, X-ray diffraction was used to characterise the cathodes before and after discharge in an Al-S cell (Figure 10). The diffraction pattern of the pristine electrode clearly shows the presence of crystalline sulfur. Then, the electrode was discharged in an EMIMCl-$AlCl_3$ electrolyte, after which the battery was disassembled inside an argon glovebox and the discharged cathode was placed in an air-tight XRD sample holder. In the diffraction pattern of the discharged electrode, all the peaks associated to crystalline sulfur have disappeared, indicating that all the sulfur has been consumed in the electrochemical discharge reactions. The pattern only contains two broad peaks, that are due to the sample holder, and three very small peaks that are unidentifiable. Therefore, the XRD data suggest that the discharge reaction consumes all the sulfur and produces no crystalline degradation products. Unfortunately, formation of crystalline Al_2S_3 is also not observed, which could be because Al_2S_3 is formed in amorphous form or because the amount of crystalline Al_2S_3 formed in the present experiments is below the limit of detection. Indeed, previous studies of Al-S batteries have also been unable to identify formation of crystalline Al_2S_3 by XRD of the discharged electrodes.[4a, 8] The high reactivity of Al_2S_3 and the electrolyte with trace amounts of water also makes the characterisation of the discharged electrodes particularly challenging, and requires special transfer sytems with stringent water-free atmosphere conditions.[25]

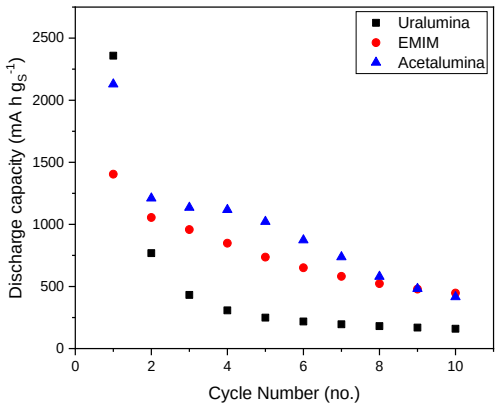

Figure 9. Discharge capacity versus cycle number data for the thin cathode coatings shown in Figure 1.

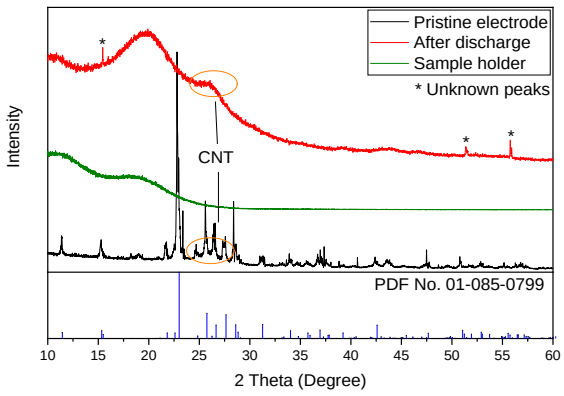

Figure 10. Powder diffraction pattern (grazing incidence, incident angle of 5°) of a sulfur cathode of 110 µm cathode thickness, in the pristine state (black line) and after a full discharge to 0.05 V (red line). The diffraction pattern of crystalline sulfur (blue line) is also shown for comparison, as well as the diffraction pattern of the sample holder (green line).

Conclusion

A systematic study of the effect of the sulfur cathode thickness on the electrochemical response of Al-S batteries is presented, for three relevant electrolytes: the most popular EMIMCl-$AlCl_3$ and two deep eutectic electrolytes made by mixing either acetamide or urea with $AlCl_3$. For the deep eutectic electrolytes, a very dramatic decrease in capacity with the sulfur cathode thickness is observed, which is attributed to the high viscosity of these electrolytes, which hampers full sulfur utilisation due to slow electrolyte ion transport within the porous electrode. SEM characterisation of the cathodes show that their morphology is not ideal, with big cracks and agglomeration of particles for the thicker cathodes, thus explaining the slow electrolyte ion transport through those packed agglomerates. Impedance measurements in symmetrical cells demonstrate that the resistance associated to electrolyte ion transport markedly increases as the cathodes are made thicker, and analysis of the results reveals that the cathode have high effective tortuosity for electrolyte ion transport, thus supporting the hypothesis that slow electrolyte ion transport limits the capacity achievable with these cathode structures. The electrochemical results of Al-S cells also show that very high capacities are obtained with the deep eutectic electrolytes with very thin sulfur cathodes, with values of specific capacity exceeding the theoretical limit of 1672 mAh g_S^{-1} expected for full reduction of sulfur to sulfide. An analysis of the electrochemical response obtained with carbon electrodes with no sulfur shows that the contribution of the capacity due to carbon is only minor. Therefore, the high specific capacity values are explained by the presence of side reactions (electrolyte degradation) that co-occur with the sulfur electrochemical reactions. On the other hand, XRD characterisation of the pristine and discharged electrode in EMIMCl-$AlCl_3$ suggest that the discharge reaction consumes all the sulfur and produces no crystalline degradation products.

In summary, this work demonstrates that the systematic study of Al-S cell performance as a function of the sulfur cathode thickness is a very powerful approach to identify and quantify issues with electrolyte degradation or limitations due to mass transport, and the approach can be easily applied to study new cathode and electrolyte formulations beyond the state of the art of the Al-S battery system.

Experimental Section

Cathode Preparation

Sulfur (Aldrich) and multi-walled carbon nanotubes (CNT, 98 % basis, Sigma-Aldrich) were mixed (in a mass ratio of 2:1, sulfur:carbon) by pestle and mortar before being transferred into a 23 ml polytetrafluoroethylene (PTFE)-lined autoclave (Parr Instrument Company). The autoclave was then placed into a preheated oven (Genlab Ltd. MINO/6, 155 °C, 6.5 hours) to allow sulfur impregnation to occur. After cooling down to room temperature, a black powder was collected. Polyethylene oxide (PEO, 600,000 M_w, Sigma-Aldrich) and polyvinylpyrrolidone (PVP, 40,000 M_w, Aldrich) were used as binder (mass ratio of PEO: PVP of 2:1, ~12 % wt. overall within the coating) and dissolved in a mixture of acetonitrile (HiPerSolv, ACS) and ethanol (Fisher, >=99.8 % analytical grade) in a 2:1 volume ratio respectively, under a fumehood. The PEO/PVP combination has been used before in Li-S batteries, and it is employed here because it provides good dispersion and mechanical stability.[22a, 26] The sulfur impregnated CNT were added into the binder solution and stirred with a stirring bar for either 2 hours or 3 days. A pre-cut piece of Mo foil (25 µm thickness, ≥ 99.9 % trace metals basis, Sigma-Aldrich) was cleaned using ethanol, before being coated with ink using a doctor blade coater. After the acetonitrile and ethanol had evaporated, the coated electrode sheet was cut into round discs (Ø = 11 mm, Hohsen hand-held precision punch). The discs were placed into a Büchi tube and dried at room temperature (typically, 20-25 °C), under vacuum for no less than 2 days. Each electrode was weighed (OHAUS Adventurer™, AR0640) inside an Ar-filled glovebox (H_2O ≤ 4.0 ppm, O_2 ≤ 0.1 ppm) before use, to obtain the precise weight of the active material. The standard electrode composition was 58.8:29.4:7.9:3.9 (S: CNT: PEO: PVP, wt.) for simplicity, this will be referred to as 60 % sulfur. A standard coating using the procedure above would use 1.4 ml acetonitrile and 0.7 ml ethanol, and when combined with a 300 µm doctor blade setting can produce a coating thickness of ~65 µm.

The cathode coating thickness was systematically varied in two ways: (i) using different settings for the wet thickness on the doctor blade coating apparatus to change the amount of ink coated, or (ii) by varying the solvent quantity in the ink thereby producing thinner/thicker coatings. Additional experiments were performed with electrodes with very small mass loading (that is, very thin cathode coatings). In order to reliably determine the cathode mass loading in these electrodes (and, thus, the sulfur loading), the coatings were made on thinner Mo foils (10 µm, 99.9 % purity, Sigma-Aldrich). The Mo foils were punched into 11 mm-diameter discs, which were pre-weighted before coating and then after coating and drying. The thinner Mo discs typically weighted between 9.9-10.1 mg while the cathode loading mass for the thin coatings was around 0.7-0.8 mg. The balance error is ±0.05 mg, which produces an error in the mass of the coating of ±0.07 mg, and therefore, the error in the reported specific capacities is ≤ 10%.

Additional results from other experimental electrodes are also reported and are labelled as “containing additives”. The additives used were TIMCAL C65, graphene nanoplates (Ossila Ltd.) or acetylene black (50 % compressed, Shawinigan Black, Chevron Phillips Chemical Company LP.) and typically between 1-8 % wt. Among the results of electrodes with additives, in a few cases the electrodes contain 50 wt. % sulfur rather than 60 wt. %.

The thicknesses of the cathode coatings on the Mo foil were measured with an ABS Digital Thickness Gauge (resolution: 1 µm). All electrodes were numbered and packaged separately.

CHNS elemental analysis carried out by MEDAC ltd., demonstrated that there had been no sulfur loss during the impregnation step, a 2:1 sulfur-to-carbon ratio was observed after the impregnation (Table S1). Additionally, no sulfur loss was noticed during the drying procedure of the

electrodes in a Büchi line at room temperature, and no significant change in the mass of the electrodes before and after drying was observed. Additionally, Transmission Electron Microscopy (TEM images taken on a Hitachi 7700 TEM at 100 kV, Figure S3) of the carbon nanotubes show that the impregnation process does not deform the structure.

Electrolyte Preparation

1-Ethyl-3-methylimidazolium chloride-aluminium chloride (EMIMCl-$AlCl_3$, 1:1.5 molar ratio) was purchased from Sigma-Aldrich. Acetalumina (acetamide: $AlCl_3$ = 1:1.5 molar ratio) and Uralumina (urea: $AlCl_3$ = 1:1.5 molar ratio) were generously provided by Dr. Christopher Zaleski (Scionix Ltd.), Dr. Igor Efimov and Prof. Karl Ryder (University of Leicester). The electrolytes were used as received.

Cell Construction

The electrochemical cells were made of materials that are resistant against corrosion in contact with the electrolytes. Preliminary experiments were conducted with Swagelok cells made of PTFE, and it was later found that Swagelok cells made of aluminium produced the same results (Figure S5, supplementary information). Although aluminium corrodes at high potentials, it is possible to use the cell body made of aluminium since the cell body is electrically disconnected from both electrodes (anode and cathode), and therefore, it remains at the open circuit potential where aluminium is stable. The cell was sealed with PFA ferrules, and Mylar film was used to line the inside of the Al cell body, thus preventing the electrodes to get in contact with the cell body. Sulfur electrodes (11 mm diameter discs) were used as cathodes, high purity Al discs (0.2 mm thick, Puratronic, 99.997 % metals basis, 11 mm diameter discs) were used as anodes. Two Whatman GF/F glass microfiber filters (12 mm diameter discs) were used as separators and, 120 µL of electrolyte were added to the cell. The pipette tips used were Solvent Safe^{TM} 200 pipet tips due to their increased resistance to acidic environments over conventional pipette tips. An aluminium bar (purity ≥97.5 %) was used as the current collector for the Al anode and a tungsten bar (purity ≥99 %) was used as current collector for the cathode. Prior to cell assembly, all the cell components were washed in ethanol (Fisher, >=99.8 % analytical grade), sonicated (Cole-Parmer, 08891-26) for 15 minutes and dried in an oven (Genlab E3, E3DWC100/N) at 80 °C. Prior to drying, the cells were partially assembled and checked for short-circuiting with a multimeter. After drying, all the components were transferred into an Ar-filled glovebox (H_2O ≤ 4.0 ppm, O_2 ≤ 0.1 ppm). The electrodes were directly transferred to the glovebox inside a Büchi tube to avoid air exposure. Cells assembly was done inside the glovebox.

Electrochemical Testing and Characterisation

After assembly inside the glovebox, the cells were placed in a Memmert climactic chamber set to 25 °C for the electrochemical characterisation. The cells were allowed to equilibrate for 6 hours and then galvanostatic cycling with potential limitation (GCPL) experiments were done applying a lower and upper voltage limit of 0.05 V and 1.85 V, respectively, using a VMP3 potentiostat (BioLogic Science Instruments). The applied specific current (normalized to the mass of sulfur) was 50 mA g_S^{-1}. Discharge to 0.05 V was done first, followed by charge to 1.85 V, and the cells were cycled for 10 cycles. Potentiostatic Impedance Spectroscopy (PEIS) measurements were carried out in symmetrical cell configuration (i.e., using two sulfur electrodes with almost identical weight and tungsten bars as current collectors, see Figure S4 in the supplementary Information). The PEIS measurements were carried out with a voltage amplitude of 10 mV and frequencies of 200 kHz - 10 mHz. The X-ray diffraction (XRD) patterns were recorded at room temperature with Rigaku Smartlab Diffractometer (Rigaku Corporation) using Cu K_α radiation operated at 45 kV, 150 mA. Samples were placed in a special X-ray transparent dome-shaped sample holder for air-sensitive materials purchased from Bruker (Ø 55.5 mm PMMA disc with Ø 25 mm x 1 mm specimen well). A piece of glass was used as a flat surface to elevate the electrode during measurements. The morphology and element distribution of raw materials and sulfur electrodes was studied using a JEOL manufactured JSM59 scanning electron microscope (SEM, 15 kV) with an Oxford instruments energy-dispersive X-ray (EDX) attachment. Viscosity measurements were taken using a Cannon-Fenske viscometer tube (Sigma-Aldrich) and the experiment was recorded using a mobile phone camera (Samsung Galaxy S10+). The viscosity values were calculated from the times the electrolytes required to flow between two marks in the viscometer, as estimated from the video.

Acknowledgements

The authors acknowledge the financial support for this work from the European Commission through the Horizon 2020 FEP-OPEN project SALBAGE (Grant agreement ID: 766581). We also thank Dr. Christopher Zaleski (Scionix Ltd.), Dr. Igor Efimov and Prof. Karl Ryder (University of Leicester) for providing two of the electrolytes used in this study, all members of the SALBAGE project and Dr. Imanol Landa-Medrano for fruitful scientific discussions, the University of Southampton X-ray diffraction unit, the Biomedical Imaging Unit, Southampton University Hospital and Mr Nikolay Zhelev (lab technician) for his assistance with data collections. NGA thanks the EPSRC for an early career fellowship (EP/N024303/1). The data for this article are available from the University of Southampton at https://doi.org/10.5258/SOTON/D1326. RR would like to dedicate his contribution to this paper to the memory of Prof. Roberto Marassi.

Keywords: Aluminum/Sulfur batteries; Electrochemistry; Energy Storage; Electrolytes; Reaction Mechanisms

[1] a) E. A. Olivetti, G. Ceder, G. G. Gaustad, X. Fu, *Joule* **2017**, *1*, 229-243; b) J.-M. Tarascon, *Nat Chem* **2010**, *2*, 510-510.
[2] J. B. Goodenough, Y. Kim, *Chemistry of Materials* **2010**, *22*, 587-603.
[3] a) M. S. Whittingham, *Chemical Reviews* **2004**, *104*, 4271-4302; b) G. Harper, R. Sommerville, E. Kendrick, L. Driscoll, P. Slater, R. Stolkin, A. Walton, P. Christensen, O. Heidrich, S. Lambert, A. Abbott, K. Ryder, L. Gaines, P. Anderson, *Nature* **2019**, *575*, 75-86.
[4] a) T. Gao, X. Li, X. Wang, J. Hu, F. Han, X. Fan, L. Suo, A. J. Pearse, S. B. Lee, G. W. Rubloff, K. J. Gaskell, M. Noked, C. Wang, *Angew Chem Int Ed Engl* **2016**, *55*, 9898-9901; b) G. A. Elia, K. Marquardt, K. Hoeppner, S. Fantini, R. Lin, E. Knipping, W. Peters, J. F. Drillet, S. Passerini, R. Hahn, *Adv Mater* **2016**, *28*, 7564-7579.
[5] a) S. H. Chung, A. Manthiram, *Adv Mater* **2019**, *31*, e1901125; b) X. Hong, J. Mei, L. Wen, Y. Tong, A. J. Vasileff, L. Wang, J. Liang, Z. Sun, S. X. Dou, *Adv Mater* **2019**, *31*, e1802822.
[6] a) D. Eroglu, K. R. Zavadil, K. G. Gallagher, *Journal of The Electrochemical Society* **2015**, *162*, A982-A990; b) M. Hagen, D. Hanselmann, K. Ahlbrecht, R. Maça, D. Gerber, J. Tübke, *Advanced Energy Materials* **2015**, *5*, 1401986.
[7] a) H. Sun, W. Wang, Z. Yu, Y. Yuan, S. Wang, S. Jiao, *Chem Commun (Camb)* **2015**, *51*, 11892-11895; b) Y. Oh, G. Lee, Y. Tak, *ChemElectroChem* **2018**, *5*, 3348-3352.
[8] G. Cohn, L. Ma, L. A. Archer, *Journal of Power Sources* **2015**, *283*, 416-422.
[9] X. Yu, A. Manthiram, *Advanced Energy Materials* **2017**, *7*.
[10] X. Yu, M. J. Boyer, G. S. Hwang, A. Manthiram, *Chem* **2018**, *4*, 586-598.
[11] H. Yang, L. Yin, J. Liang, Z. Sun, Y. Wang, H. Li, K. He, L. Ma, Z. Peng, S. Qiu, C. Sun, H. M. Cheng, F. Li, *Angew Chem Int Ed Engl* **2018**, *57*, 1898-1902.
[12] Y. Bian, Y. Li, Z. Yu, H. Chen, K. Du, C. Qiu, G. Zhang, Z. Lv, M.-C. Lin, *ChemElectroChem* **2018**, *5*, 3607-3611.
[13] W. Wang, Z. Cao, G. A. Elia, Y. Wu, W. Wahyudi, E. Abou-Hamad, A.-H. Emwas, L. Cavallo, L.-J. Li, J. Ming, *ACS Energy Letters* **2018**, *3*, 2899-2907.
[14] W. Chu, X. Zhang, J. Wang, S. Zhao, S. Liu, H. Yu, *Energy Storage Materials* **2019**, *22*, 418-423.
[15] K. Zhang, T. H. Lee, J. H. Cha, R. S. Varma, J. W. Choi, H. W. Jang, M. Shokouhimehr, *Sci Rep* **2019**, *9*, 13573.
[16] a) J. S. Wilkes, J. A. Levisky, R. A. Wilson, C. L. Hussey, *Inorganic Chemistry* **1982**, *21*, 1263-1264; b) P. K. Lai, M. Skyllas-Kazacos,

Journal of Electroanalytical Chemistry and Interfacial Electrochemistry **1988**, *248*, 431-440; c) P. R. Gifford, *Journal of The Electrochemical Society* **1988**, *135*, 650.

[17] a) J. S. Wilkes, J. S. Frye, G. F. Reynolds, *Inorganic Chemistry* **1983**, *22*, 3870-3872; b) Z. J. Karpinski, R. A. Osteryoung, *Inorganic Chemistry* **1984**, *23*, 1491-1494; c) A. A. Fannin, L. A. King, J. A. Levisky, J. S. Wilkes, *The Journal of Physical Chemistry* **1984**, *88*, 2609-2614; dC. L. Hussey, *Journal of The Electrochemical Society* **1986**, *133*, 1389.

[18] a) H. M. A. Abood, A. P. Abbott, A. D. Ballantyne, K. S. Ryder, *Chemical Communications* **2011**, *47*, 3523-3525; b) A. P. Abbott, R. C. Harris, Y.-T. Hsieh, K. S. Ryder, I. W. Sun, *Physical Chemistry Chemical Physics* **2014**, *16*, 14675-14681; c) M. Angell, C. J. Pan, Y. Rong, C. Yuan, M. C. Lin, B. J. Hwang, H. Dai, *Proc Natl Acad Sci U S A* **2017**, *114*, 834-839; d) N. Canever, N. Bertrand, T. Nann, *Chem Commun (Camb)* **2018**, *54*, 11725-11728; e) H. Jiao, C. Wang, J. Tu, D. Tian, S. Jiao, *Chem Commun (Camb)* **2017**, *53*, 2331-2334; f) C. Zhang, Y. Ding, L. Zhang, X. Wang, Y. Zhao, X. Zhang, G. Yu, *Angewandte Chemie International Edition* **2017**, *56*, 7454-7459.

[19] a) F. Coleman, G. Srinivasan, M. Swadźba-Kwaśny, *Angewandte Chemie International Edition* **2013**, *52*, 12582-12586; b) C. Liu, W. Chen, Z. Wu, B. Gao, X. Hu, Z. Shi, Z. Wang, *Journal of Molecular Liquids* **2017**, *247*, 57-63; c) P. Hu, R. Zhang, X. Meng, H. Liu, C. Xu, Z. Liu, *Inorganic Chemistry* **2016**, *55*, 2374-2380.

[20] a) M. Lipsztajn, *Journal of The Electrochemical Society* **1983**, *130*, 1968; b) M. Lipsztajn, R. A. Osteryoung, *Inorganic Chemistry* **1984**, *23*, 1735-1739; c) Z. J. Karpinski, R. A. Osteryoung, *Inorganic Chemistry* **1985**, *24*, 2259-2264.

[21] a) S. Drvarič Talian, G. Kapun, J. Moškon, A. Vizintin, A. Randon-Vitanova, R. Dominko, M. Gaberšček, *Chemistry of Materials* **2019**, *31*, 9012-9023; b) T. Zhang, M. Marinescu, S. Walus, P. Kovacik, G. J. Offer, *Journal of The Electrochemical Society* **2017**, *165*, A6001-A6004; c) Y.-C. Chien, A. S. Menon, W. R. Brant, D. Brandell, M. J. Lacey, *Journal of the American Chemical Society* **2020**, *142*, 1449-1456.

[22] a) M. J. Lacey, V. Österlund, A. Bergfelt, F. Jeschull, T. Bowden, D. Brandell, *ChemSusChem* **2017**, *10*, 2758-2766; b) A. Jozwiuk, H. Sommer, J. Janek, T. Brezesinski, *Journal of Power Sources* **2015**, *296*, 454-461.

[23] a) R. Raccichini, L. Furness, J. W. Dibden, J. R. Owen, N. García-Araez, *Journal of The Electrochemical Society* **2018**, *165*, A2741-A2749; b) R. Raccichini, M. Amores, G. Hinds, *Batteries* **2019**, *5*, 12.

[24] a) M. Gaberscek, J. Moskon, B. Erjavec, R. Dominko, J. Jamnik, *Electrochemical and Solid-State Letters* **2008**, *11*, A170; b) S. Dsoke, X. Tian, C. Täubert, S. Schlüter, M. Wohlfahrt-Mehrens, *Journal of Power Sources* **2013**, *238*, 422-429; c) J. Landesfeind, J. Hattendorff, A. Ehrl, W. A. Wall, H. A. Gasteiger, *Journal of The Electrochemical Society* **2016**, *163*, A1373-A1387; d) J. Landesfeind, D. Pritzl, H. A. Gasteiger, *Journal of The Electrochemical Society* **2017**, *164*, A1773-A1783; e) A. S. Keefe, S. Buteau, I. G. Hill, J. R. Dahn, *Journal of The Electrochemical Society* **2019**, *166*, A3272-A3279.

[25] a) T. Welton, *Chemical Reviews* **1999**, *99*, 2071-2084; b) J. Estager, J. D. Holbrey, M. Swadźba-Kwaśny, *Chemical Society Reviews* **2014**, *43*, 847-886; c) G. Zampardi, F. La Mantia, *Batteries & Supercaps* **2020**, *3*, 1-27.

[26] a) M. J. Lacey, F. Jeschull, K. Edström, D. Brandell, *Journal of Power Sources* **2014**, *264*, 8-14; b) Z. W. Seh, Q. Zhang, W. Li, G. Zheng, H. Yao, Y. Cui, *Chemical Science* **2013**, *4*, 3673-3677.

Entry for the Table of Contents

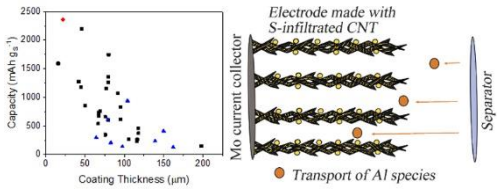

The rate of transport of Al-containing electrolyte species and electrolyte degradation are critical for the development of Al-S batteries.